International Journal of Hydrogen Energy 203 (2026) 153172

Contents lists available at ScienceDirect

International Journal of Hydrogen Energy

journal homepage: www.elsevier.com/locate/he

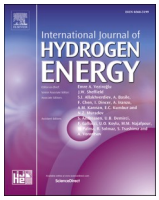

CBAM-aligned dynamic techno-economic optimization of renewable hydrogen systems

Metin Gül [a,c,*], Ersin Akyüz [b,c]

[a] Department of Electrical and Energy, Balıkesir Vocational School, Balıkesir University, 10145, Balıkesir, Türkiye
[b] Department of Electrical and Electronics Engineering, Faculty of Engineering, Balıkesir University, 10145, Balıkesir, Türkiye
[c] Renewable Energy Research and Application Center, Balıkesir University, 10145, Balıkesir, Türkiye

ARTICLE INFO

Keywords:
Techno-economic analysis
Multi-objective optimization
Dynamic simulation
Break-even analysis
NSGA-III
MOPSO

ABSTRACT

This study presents a comprehensive techno-economic framework for evaluating 20-year green hydrogen production from grid-connected PEM electrolyzers powered by hybrid PV–WT systems. Rather than introducing new modelling or optimization techniques, the contribution lies in integrating detailed dynamic Simulink simulation, long-term component degradation, water sourcing and treatment costs, and hydrogen storage pathways within a unified, policy-aligned assessment. Using hourly PPA-based electricity prices for Türkiye, the framework combines ANN surrogate modelling with MOPSO and NSGA-III to identify Pareto-optimal system sizes that balance the levelized cost of hydrogen (LCOH) and renewable fraction (RenFrac). Site-specific results indicate that Bandırma and Çeşme favour MOPSO for robust low-cost configurations (LCOH ≈ 5.3–5.5 USD/kg, RenFrac ≈ 0.9), while Mersin is better represented by NSGA-III (6.5 USD/kg, 0.85). Sensitivity analyses show CAPEX and discount rate as primary cost drivers, whereas strategically aligning electrolyzer downtime with evening high-price hours enhances competitiveness. Economies of scale reduce LCOH by up to 40 % between 1 MW and 50 MW, with financial breakeven near 7.2 USD/kg and viable returns at ≥ 8 USD/kg. Overall, the framework provides actionable insights for project developers and policymakers, particularly in the context of CBAM and Türkiye's 2053 net-zero pathway.

1. Introduction

The rising worldwide demand for energy, the progressive depletion of fossil fuel resources, and the urgent imperative to reduce greenhouse gas emissions have driven increasing interest in hybrid renewable energy systems (HRESs) for distributed generation. These systems typically combine photovoltaic (PV) and wind turbine (WT) systems as their primary energy sources [1]. Yet, the inherent intermittency and variability of renewable energy sources (RES) create challenges in maintaining a stable and continuous power supply, which necessitates the support of backup generation units or energy storage systems (ESS) [2]. Hydrogen has been widely examined as part of renewable-integrated energy systems, and numerous studies have assessed its technical and economic performance under varying assumptions [3,4].

Although green hydrogen offers significant benefits, its production cost is still considerably higher than that of traditional grey hydrogen. In addition, the estimation process depends on numerous technical, economic, and operational parameters; however, prior cost assessments show substantial variation due to differences in assumptions regarding CAPEX, electricity pricing, renewable resource quality, and electrolyzer performance [3]. This highlights the necessity of conducting detailed cost assessments. These evaluations are crucial both for determining the present production costs of green hydrogen and for estimating when it might achieve price parity with grey hydrogen, which is currently around US$1–2 per kilogram of H_2 [4–6].

Previous techno-economic studies have consistently shown that hydrogen costs are strongly influenced by capital expenditure, renewable capacity factors, electricity pricing structures, and discount rate assumptions [7]. Several works highlight the dominant role of discount rate variability and renewable resource quality in shaping LCOH outcomes [8,9], while others demonstrate that water sourcing and storage configurations can also shift long-term costs [10,11]. Although additional studies examine PEM electrolyzer systems under different market or design assumptions [12–14], these analyses typically rely on one-year

This article is part of a special issue entitled: IHTEC-2025 (Colpan) published in International Journal of Hydrogen Energy.

* Corresponding author. Department of Electrical and Energy, Balıkesir Vocational School, Balıkesir University, 10145, Balıkesir, Türkiye.
E-mail address: metingul@balikesir.edu.tr (M. Gül).

https://doi.org/10.1016/j.ijhydene.2025.153172
Received 24 September 2025; Received in revised form 6 December 2025; Accepted 20 December 2025
Available online 26 December 2025
0360-3199/© 2025 Hydrogen Energy Publications LLC. Published by Elsevier Ltd. All rights are reserved, including those for text and data mining, AI training, and similar technologies.

simulations and evaluate only a limited subset of sensitivity parameters, leaving broader multi-factor interactions underexplored.

Despite these contributions, prior studies typically examine electrolyzer performance, renewable variability, water sourcing, or storage effects in isolation. Existing analyses rarely integrate long-term component degradation, water treatment requirements, storage pathways, and hourly market-based operation within a unified optimization framework. This combined gap motivates the integrated modelling approach adopted in the present study.

Recent global assessments, such as the IEA Global Hydrogen Review 2024, indicate that low-emission hydrogen still constitutes a marginal share of total production (below 1 Mt in 2023), underscoring persistent cost and demand barriers [15]. Several recent techno-economic studies contribute deeper insights: Vives et al. analyze LCOH improvements via waste heat recovery and ORC integration [16], while Curcio (2025) provides a comparative cost outlook for grey, blue, and green hydrogen and projects that green hydrogen may reach parity at ~1 USD/kg by 2031 through policy and efficiency improvements [7]. Schofield et al. (2024) further demonstrate that incorporating electrolyzer degradation into dynamic models raises LCOH significantly in early years, though costs drop by 2030 [8]. The water costs and energy requirements of water treatments and hydrogen storage are also important on hydrogen production costs. Simões et al. [9] developed a sustainability-based framework to evaluate different water sources for electrolysis, showing that public grid water generally offers the lowest costs and risks, while seawater and wastewater face higher transport and treatment challenges. Teske et al. [10] conducted a techno-economic comparison of hydrogen storage systems versus battery storage in a real grid integration context, demonstrating practical cost trade-offs. Additionally, optimization-driven studies—such as Okonkwo et al.'s metaheuristic optimization of PV–WT–electrolyzer systems across multiple Australian cities [11], Yang et al.'s parametric optimization of solar–-wind hybrid hydrogen systems in Kuqa, China [12], and Tezer et al.'s multi-objective optimization of stand-alone PV and PV/T hybrid renewable energy systems using NSGA-II—provide valuable methodological advances [13]. A review of the literature indicates that optimization-based models often rely on simplified and empirical representations rather than employing detailed mathematical formulations of each subsystem. Moreover, no study has jointly incorporated water treatment and transport costs, long-term electrolyzer degradation, and hourly market-driven curtailment into a unified, simulation-based optimization framework. Although each of these factors, or in some cases pairs of them, has been examined individually, an optimization model that integrates all of them simultaneously is absent from the literature. These factors introduce significant challenges in the optimization process, thereby limiting the accuracy of LCOH estimations and underscoring the need for more comprehensive approaches that reflect actual operational and market conditions. Overall, existing studies highlight the inherent complexity of green hydrogen economics and emphasize the necessity of comprehensive, multi-parameter techno-economic cost analyses.

The modelling tools adopted in this study—dynamic Simulink simulation, ANN-based surrogate modelling, and multi-objective optimization—are well established in the hydrogen systems literature. Accordingly, the aim of this work is not to introduce new modelling techniques, but to integrate these components within a long-term, region-specific and policy-aligned techno-economic decision framework. This ensures that the contribution is positioned as a comprehensive applied assessment rather than a methodological innovation. Against this background, the present study develops a comprehensive techno-economic framework for grid-connected PEM electrolyzer systems powered by hybrid PV-WT configurations. The analysis employs two independent optimization algorithms to determine the optimal system sizing under real hourly market conditions using actual 2024 PPA price signals in Türkiye, thereby capturing realistic market variability. Beyond the conventional one-year horizon, this study extends the temporal scope to 175,200 operating hours (20 years), enabling a dynamic net present value (NPV) evaluation that incorporates technology degradation, discounting, and long-term investment performance. Sensitivity analyses are carried out across a broad spectrum of technical and financial factors. These include curtailment, O_2 price, taxation, discount rate, CAPEX reduction scenarios, and the degradation rates of PV, WT, and electrolyzer subsystems. Moreover, the study explicitly incorporates five distinct water sources and evaluates their treatment and supply costs, alongside both gaseous and liquid hydrogen storage options.

As summarized in Table 1, recent optimization-based studies have demonstrated significant progress in improving the techno-economic and environmental performance of hydrogen production systems. Reported LCOH values for hybrid renewable configurations generally range from 2 to 6 USD kg^{-1} H_2, depending on system scale, resource conditions, and integration strategy. While most research has focused on individual process optimization or component-level improvement, comparative studies across regions and operational strategies remain limited. In particular, dynamic operation strategies—such as flexible scheduling, off-hour management, and grid-interactive control—are

Table 1
Summary of recent optimization-based studies on green hydrogen production.

Ref	System/Method	Optimization Technique	Objective (s)	Key Quantitative Findings
[14]	Solar steam methane reforming (SMR) with molten salt	Hybrid deep neural network + multi-objective PSO	Maximize η, minimize CO_2 emissions	Achieved η = 77.5–87 %; CO_2 = 578–598 t yr^{-1}; total annual cost reduced by ~ 15 %
[17]	Solar-driven steam–autothermal hybrid reforming (SAHRP)	Multi-criteria (Aspen Plus)	Minimize CO_2 and cost; maximize η and ψ	53.4 % energy η; 45 % ψ; CO_2 reduction ≈ 97 kt yr^{-1} (≈$1.9 M tax saving)
[18]	PEM electrolyzer + SOFC integrated system	Multi-attribute (cost–CO_2–ψ)	Minimize cost and CO_2; maximize ψ	CO_2 reduced 12.9 %; power output increased 8.7 %; ψ decreased 6.3 %
[19]	PV–fuel cell (PV–FC) hybrid system	Gaussian process regression + NSGA-II	Minimize LCOH and CO_2; maximize η	CO_2 reduction ≈ 3343 t; LCOH ≈ $1.5–2 kg^{-1}; system renewable share ≈ 100 %
[20]	PV–wind–DG–Li-ion–electrolyzer hybrid	HOMER Pro + TOPSIS + VIKOR	Minimize COE, COH; maximize RenFrac	COE = $0.252 kWh^{-1}; COH = $2.59 kg^{-1}; RenFrac = 98.4 %; payback = 6.1 yr
[21]	Solar poly-generation (PVT–ORC–PEM–LNG)	NSGA-II + EES	Maximize ψ and power; minimize cost	ψ = 16.24 %; Power = 33.3 kW; cost rate = 4.48 $ h^{-1}
[22]	PV–SOFC with TIG/TEG heat recovery	HOMER Pro + sensitivity analysis	Minimize LCOH and CO_2; maximize η	LCOE = $0.108 kWh^{-1}; H_2 production = 0.28 Mt yr^{-1}; CO_2 reduced 5.6 %

rarely modelled in combination with renewable intermittency and degradation effects. Building upon these insights, the present study develops an integrated, simulation-based multi-objective optimization framework to minimize LCOH while maximizing the renewable fraction (RenFrac). This framework bridges the gap between surrogate-model optimization and full dynamic Simulink validation, providing a quantitative foundation for evaluating green hydrogen feasibility across different regional resource profiles.

In summary, previous techno-economic studies have provided valuable insights but remain limited in one or more aspects. Most short-term analyses [31–33] employ one-year static evaluations that overlook degradation and long-term investment dynamics. Others, such as Ref. [11,13], focus mainly on optimization but rely on simplified subsystem representations, omitting water treatment, compression, or storage energy penalties. Global reviews like Ref. [7,8] highlight the cost impact of electrolyzer degradation but do not embed these effects in hour-by-hour dynamic simulations. Likewise, frameworks such as Ref. [10,34] address water source and storage trade-offs in isolation, without coupling them to market-based operation or multi-objective optimization. In contrast, the present study uniquely integrates all these dimensions within a single 20-year dynamic simulation framework—linking hourly resource variability, PPA-driven electricity costs, degradation effects, and water treatment/storage costs—optimized through MOPSO and NSGA-III to ensure both techno-economic rigor and real-market applicability.

Although dynamic simulation, surrogate modelling, and multi-objective optimization are widely used in renewable hydrogen studies, existing works typically analyze these dimensions in isolation and over short horizons. Most studies rely on one-year static evaluations, simplified electrolyzer models, or omit water sourcing, storage penalties, and long-term degradation effects. Likewise, policy-oriented analyses rarely integrate CBAM-aligned fiscal mechanisms with detailed operational modelling. The contribution of this study is therefore not methodological innovation, but the development of a comprehensive and integrated techno-economic framework that jointly incorporates 20-year dynamic behaviour, degradation of PV–WT–electrolyzer subsystems, water sourcing and treatment pathways, hydrogen storage alternatives, and hourly market-based operation under policy scenarios relevant to Türkiye. To our knowledge, no previous study has combined these elements within a unified, simulation-supported optimization environment. Given Europe's CBAM framework and Türkiye's 2053 net-zero target, evaluating hydrogen production under realistic policy and fiscal conditions has become essential for determining market-aligned system feasibility.

2. Materials and methods

The methodological framework of this research (Fig. 1) establishes an integrated approach that links high-resolution technical simulations with long-term economic feasibility assessment and optimization. Previous techno-economic models for renewable-driven hydrogen systems have typically relied on static or simplified component representations—such as manufacturer power curves for wind turbines, constant-efficiency PV modules, and steady-state electrolyzer equations neglecting thermal and degradation dynamics—which limit temporal accuracy and underestimate part-load behaviour. The present study overcomes these limitations through a fully dynamic Simulink-based modelling framework that couples hourly meteorological inputs with detailed physical sub-models for each subsystem.

- The PV module is implemented via a single-diode model solved iteratively (Newton–Raphson) with NOCT-based temperature feedback and hourly degradation, enabling realistic I–V and power–temperature responses.
- The wind turbine model replaces fixed power curves with an aerodynamic $C_p(\lambda)$ formulation derived from rotor dynamics, capturing transient tip-speed effects and sub-Betz efficiency variations.
- The PEM electrolyzer incorporates electrochemical–thermal coupling: activation, ohmic, and concentration overpotentials, heat generation, transient temperature evolution, and voltage degradation every 80,000 h, resolving load-following and life-cycle effects absent in earlier works.

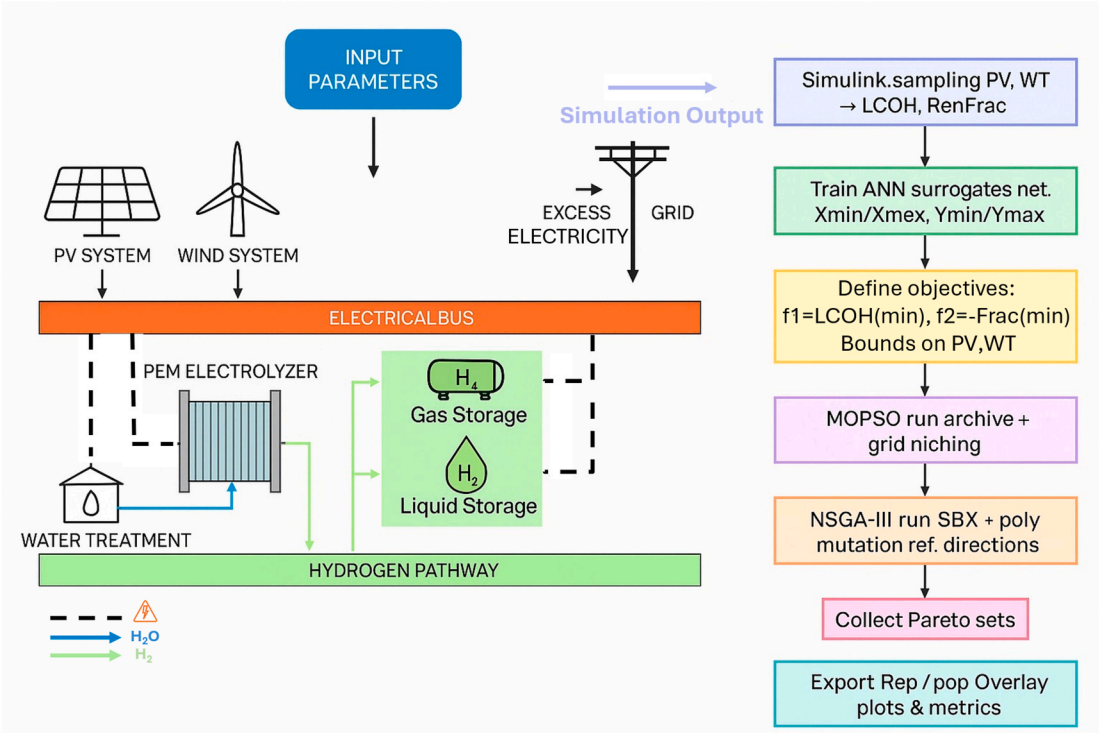

Fig. 1. System layout and optimization workflow.

- The balance-of-plant includes dynamic compressor sizing, cryogenic liquefaction energy, and explicit water-treatment CAPEX/OPEX, linking technical operation to economic outcomes.
- A long-term simulation engine connects all hourly states (175,200 h ≈ 20 years) to discounted cash flows, integrating degradation, carbon taxation, and O_2 valorization into the LCOH metric.

Collectively, these enhancements transform previously steady or semi-empirical frameworks into a physics-based, time-resolved, and financially coupled model, ensuring internal consistency between energy balances, degradation trajectories, and economic indicators. The resulting platform establishes a robust bridge between hourly technical dynamics and long-term techno-economic optimization, forming the basis for the subsequent multi-objective analysis and policy-based scenario evaluation.

Following the dynamic simulation and economic coupling, an optimization layer was implemented to systematically minimize the LCOH and maximize the RenF. To handle the high computational demand of 20-year hourly simulations, surrogate models trained on Simulink-generated datasets were employed to approximate nonlinear subsystem responses with high fidelity. Two hybrid metaheuristic algorithms—Multi-Objective Particle Swarm Optimization (MOPSO) and Non-dominated Sorting Genetic Algorithm III (NSGA-III)—were integrated to ensure both global exploration and fine-grained convergence across the Pareto front. Each optimization run co-determines the PV and WT capacities and the electrolyzer's operating schedule (start–stop hours) under hourly market prices and grid constraints. The resulting Pareto-optimal sets enable trade-off analyses between economic (LCOH, NPV) and environmental (RenF) objectives, providing decision-support insights for both technical design and policy formulation.

2.1. Technical modelling

Each subsystem is modelled in MATLAB/Simulink to provide high-resolution outputs. Simulink is a graphical simulation and model-based design environment widely used for multi-domain dynamic systems, allowing integration of electrical, mechanical, and control components within a unified framework [35]. Three representative sites—Bandırma, Çeşme, and Mersin—were selected to capture distinct renewable resource and market characteristics across Türkiye: a wind-dominated region (Çeşme), a solar-rich inland location (Mersin), and a balanced hybrid coastal zone (Bandırma). This geographic diversity enables evaluation of system behaviour under varying PV–wind complementarities and grid conditions. The PV and WT models yield hourly renewable electricity production based on meteorological inputs. This site selection strategy was intentionally designed to represent diverse renewable resource conditions, thereby demonstrating the adaptability of the proposed techno-economic framework. Since all major subsystems (PV, WT, electrolyzer, storage, and grid interface) were parameterized through climate- and cost-dependent inputs, the same methodology can be directly extended to other regions or countries with distinct renewable energy profiles. Hourly meteorological data required for the simulations, including global horizontal irradiance (ALLSKY_SFC_SW_DWN), air temperature at 2 m (T2M), and wind speed at 50 m (WS50 M), were obtained from the NASA POWER Data Access Viewer/API (Renewable Energy community) [36] for three locations in Turkey: Bandırma (40.35° N, 27.97° E), Çeşme (38.32° N, 26.30° E), and Mersin (36.80° N, 34.63° E).The PEM electrolyzer model calculates stack voltage, power consumption, hydrogen mass flow rate, and water balance. Compression and water treatment units are modelled to reflect both electricity consumption and operational constraints. All subsystems are integrated into a system-wide energy balance, where surplus electricity is exported to the grid and deficits are met through imports. The operational schedule, defined by start and stop hours, governs the effective utilization of the electrolyzer and forms the basis for computing the capacity factor and renewable fraction.

2.1.1. Photovoltaic subsystem

The PV subsystem is modelled using a modified single-diode equivalent circuit approach, which accounts for irradiance, ambient temperature, and module efficiency. Hourly irradiance and temperature data are incorporated into the model to reflect seasonal and diurnal variability. The model outputs the instantaneous current–voltage (I–V) characteristics of the array and determines the maximum power point (MPP) at each time step. Array scaling is performed based on the number of modules connected in series. Further details of the mathematical formulations, including diode equation parameters and temperature correction factors, are provided in Appendix A1.1.

Fig. 2 presents the monthly mean values of solar radiation (a) and ambient temperature (b) for Mersin, Çeşme, and Bandırma, based on hourly data. The polar plots highlight the seasonal variation across the three sites: Mersin exhibits the highest radiation and temperature values, Çeşme shows moderate values, while Bandırma remains lower particularly during winter. These climatic differences directly influence photovoltaic generation potential and operating conditions of the PV subsystem.

2.1.2. Wind turbine subsystem

The wind turbine subsystem is modelled based on the turbine-specific power curve approach, which links hub-height wind speed to electrical power output through aerodynamic and mechanical conversion efficiencies. The model accounts for the fundamental parameters of wind energy conversion, including air density, rotor swept area, turbine power coefficient, and drivetrain efficiency. Cut-in, rated, and cut-out wind speeds are incorporated to define the operational envelope of the turbine. Hourly wind speed data were adjusted to hub height using a logarithmic wind profile, while the turbine power output was subsequently calculated by applying the characteristic power curve. The complete mathematical formulations for the WT model, including the aerodynamic power equation, hub-height wind speed adjustment, and efficiency terms, are provided in Appendix A1.2.

To capture the temporal variability of the wind resource, site-specific hourly wind speed datasets were used for Mersin, Çeşme, and Bandırma. Fig. 3 presents the two-dimensional distributions of mean wind speed as a function of both month and hour of the day for the three locations. The plots highlight the distinctive seasonal and diurnal characteristics of each site: Mersin exhibits higher variability with summer peaks, Çeşme shows relatively stable and strong wind patterns across the year, while Bandırma displays moderate seasonal dependence with pronounced afternoon maxima. These datasets were integrated into the WT model to ensure accurate representation of local wind regimes in subsequent system simulations.

2.1.3. Hydrogen production plant

2.1.3.1. Balance of plant (BOP). The BOP includes compressors, pumps, and auxiliary components. Compressors are modelled using isentropic relations, with energy consumption determined by pressure ratio, isentropic efficiency, and mechanical efficiency. Water treatment requirements are modelled based on source-dependent energy consumption and treatment steps, such as filtration, desalination, or deionization, depending on the assumed water source. Auxiliary electrical loads are aggregated into the system-level energy balance. Details of compressor power calculations and water treatment energy models are given in Appendix A1.4.

2.1.3.2. PEM electrolyzer. "In this study, a PEM electrolyzer is considered, as its capability of rapid start-up and shutdown makes it highly suitable for flexible and dynamic operation [37]. The PEM electrolyzer is modelled at the stack level using an approach that accounts for electrochemical voltage, activation overpotential, ohmic losses, and concentration losses. The model captures dynamic hydrogen production

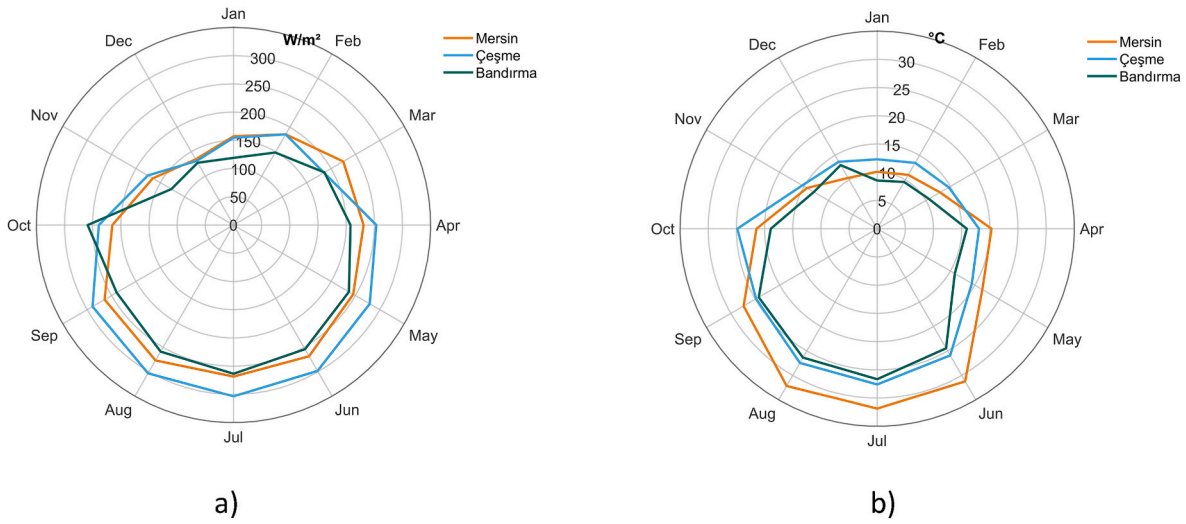

Fig. 2. Monthly solar radiation and temperature profiles for Mersin, Çeşme, and Bandırma.

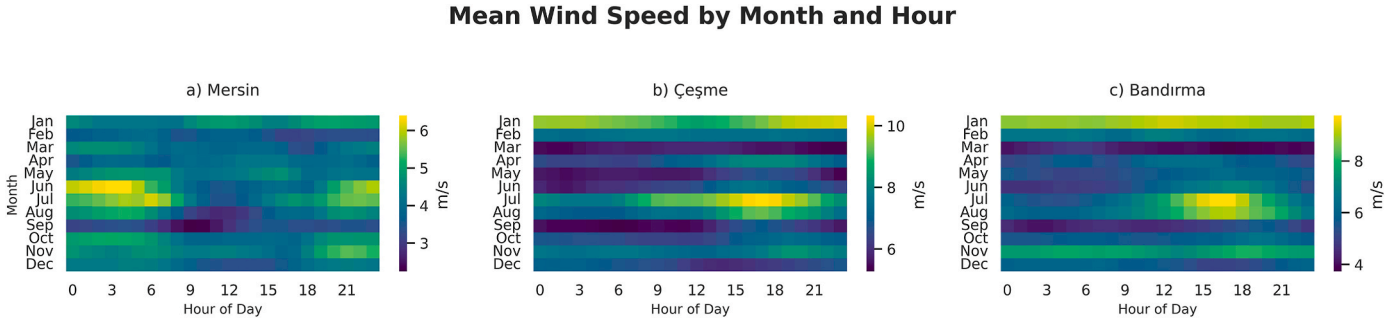

Fig. 3. Monthly–hourly wind speed distributions for a) Mersin, b) Çeşme, and c) Bandırma.

rates through Faraday's law, linking stack current to hydrogen mass flow. Temperature-dependent parameters such as membrane conductivity and efficiency are considered. In addition to electrical behaviour, the electrolyzer model incorporates species balances for hydrogen, oxygen, and water, ensuring that mass conservation is satisfied. The detailed set of equations is presented in Appendix A1.3.

Fig. 4 presents an illustrative representation of the efficiency and hydrogen production of the simulated PEM electrolyzer under operating conditions of 80 °C and 30 bar, provided for informational purposes.

2.1.3.3. Hydrogen storage. In this study, the hydrogen storage is considered in both compressed gaseous and liquid forms for comparison.

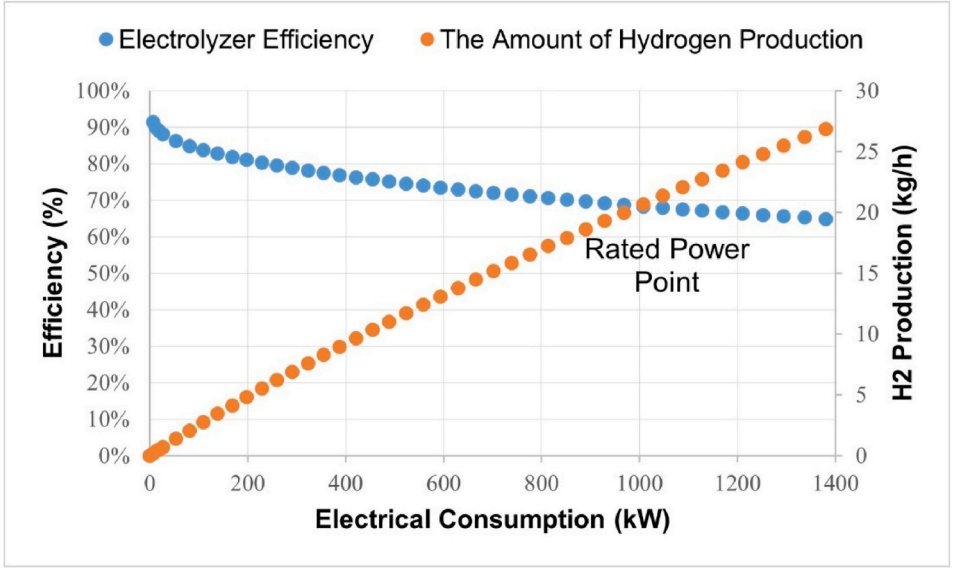

Fig. 4. PEM electrolyzer efficiency and hydrogen production versus electrical consumption.

For compressed storage, the energy demand of multistage compression and cooling is included. For liquid storage, the cryogenic liquefaction model incorporates precooling, expansion, and ortho-para conversion energy requirements. Storage efficiencies and boil-off losses are also considered. The mathematical formulation of storage energy demands is summarized in Appendix A1.4.2 and A1.4.3.

2.2. Economical modelling

The economic model is structured as a 20-year discounted cash flow framework. It explicitly includes.

- **CAPEX:** PV plant, WT, electrolyzer stacks and balance-of-plant, hydrogen storage (compressed and liquid), compressors, and water intake/treatment facilities.
- **OPEX:** routine maintenance, electrolyzer stack replacements (every 80,000 h), auxiliary loads (pumps, heaters, cooling), water sourcing and treatment costs A1.1.5, and grid electricity imports.
- **Revenues and adjustments:** grid electricity sales under PPA, oxygen by-product valorization, and taxation on net income (including carbon tax on grid imports).

The central performance metric is the LCOH, defined as [38]:

$$LCOH = \frac{CAPEX + \sum_{t=1}^{N} \left(\frac{OPEX_t + E_{import,t} - E_{export,t} - Rev_{O_{2,t}} + Tax_t}{(1+r)^t} \right)}{\sum_{t=1}^{N} \frac{H_{2,t}}{(1+r)^t}} \quad (1)$$

where N = 20 years, r is the discount rate, and $H_{2,t}$ is the hydrogen output in year t.

Net Present Value (NPV):

$$\mathrm{NPV} = \sum_{t=1}^{N} \frac{CF_t}{(1+r)^t} \quad (2)$$

Where CF_t is Cash Flow at time *t*.

- **IRR:** the discount rate r* for which NPV = 0.
- **Payback Period:** the year in which cumulative discounted cash flows first become positive.

$$PBP = min\left\{ t \middle| \sum_{t=1}^{N} \frac{CF_t}{(1+r)^t} \right\} \geq 0 \quad (3)$$

These indicators allow for evaluating both cost-competitiveness and financial feasibility. The framework also supports sensitivity analyses. The techno-economic characteristics of the PV, wind turbine, electrolyzer, compressors, storage, and water sources are summarized in Table 2, including CAPEX/OPEX scaling laws and key operating conditions.

All subsystem-specific mathematical formulations, yearly segmentation procedures, and detailed water/compression/liquefaction cost models are provided in Appendix A2 and A3.

2.2.1. Policy-driven techno-economic scenarios

To assess the fiscal and regulatory impact on hydrogen economics, five distinct policy scenarios were formulated, each modifying specific components of the base techno-economic model. The Base case assumes a constant 30 % corporate tax rate and no fiscal incentives. In the Reduced Tax scenario, the tax rate is lowered to 20 %, representing a moderate incentive for industrial hydrogen investments. The Carbon Credit case introduces an environmental subsidy equivalent to 100 USD tCO_2^{-1}, monetized according to 8.5 tCO_2 avoided per ton of hydrogen, credited annually as additional revenue. The Investment Tax Credit (ITC) applies a 20 % deduction on CAPEX in year 0, directly reducing upfront investment costs. The Accelerated Depreciation scenario implements a 20 % y^{-1} depreciation schedule during the first five fiscal years, providing a temporary tax shield through reduced taxable income. All scenarios maintain identical technical assumptions (See in Table 3), electricity price inputs (hourly PPA-based tariffs), and cost structure, enabling an isolated evaluation of fiscal policy effects on LCOH, NPV, IRR, and payback.

2.3. Optimization framework

A multi-objective optimization approach was employed to evaluate trade-offs between economic and technical performance. Decision variables included PV size, WT size, and electrolyzer operating schedule (start/stop hours). The search space for PV and WT sizes was set between 1 MW and 50 MW, reflecting both the renewable resource potential of the study regions and realistic scales for near-term deployment in

Table 2
Technical and economic parameters of system components and water sources used in the analysis.

Component	Parameter	Value/Range	CAPEX Expression	OPEX Expression	Ref.
PV	Installed capacity	1 MWp (scalable)	1.247 × (size[MW])^0.85	20.4 × size(kW)	[23]
	Annual degradation rate	0.5 %/year (scalable)			
WT	Rated power	1 MW (scalable)	1.268 × (size[MW])^0.85	28.83 × size(kW)	[24]
	Hub height	80 m			
	Cut-in/Cut-out speed	3 m/s – 25 m/s			
	Annual degradation rate	1.6 %/year (scalable)			
PEM Electrolyzer	Rated capacity	1 MW (scalable)	1.445 × (size[MW])^0.85	3 % of CAPEX	[25]
	Operating pressure	≤30 bar			
	Operating temperature	≤80 °C			
	Annual degradation rate	1 %/year (scalable)			
Gas Compressor	Outlet pressure	350–700 bar	25,958 × [kW]^0.71	3 % of CAPEX	[26]
Liquid H_2 Compressor	Outlet pressure	40 bar + cryogenic stage	Included in liquefier system	Included in liquefier system	[27]
Liquefier	–	–	5.6 × 10^6 × [kg]^0.8 × I(CEPCI)	1 % of CAPEX	[27]
H_2 Storage Tank	Type	Compressed/Liquid	520–320 $/kg storage capacity	–	[28]
	Nominal capacity	≥500 kg			
	Storage pressure (compressed)	350–700 bar			
	Storage temperature (liquid)	−253 °C			
Water Source	Tap water (TW)	CAPEX: 500,000 $; OPEX: 0	Energy: 4.50 kWh/m^3	–	[29]
	Industrial water (IW)	CAPEX: 776,000 $ + 25,000 $	Energy: 4.5635 kWh/m^3	0.18 $/$m^3$	[29]
	Groundwater (GW)	CAPEX: 580,000 $ + 150,000 $	Energy: 4.55 kWh/m^3	0.60 $/$m^3$	[29]
	Rainwater (RW)	CAPEX: 201,000 $	Energy: 0.0635 kWh/m^3	–	[29]
	Seawater (SW)	CAPEX: 576,000 $ + 80,000 $	Energy: 4.501 kWh/m^3	–	[29]
Factors	Emission factor	0.44 kg CO_2/kWh	–	–	[30]
	General taxes	30 %	–	–	

Table 3
Summary of fiscal parameters.

Parameter	Base	Reduced Tax	Carbon Credit	ITC
Corporate tax rate	30 %	20 %	30 %	30 %
Carbon price (USD/tCO_2)	–	–	100	–
Avoided CO_2 (tCO_2/tH_2)	–	–	8.5	–
Investment tax credit	–	–	–	20 % of CAPEX
Accelerated depreciation	–	–	–	20 % y^{-1} for first 5 years
Electricity pricing	PPA-based	PPA-based	PPA-based	PPA-based

Türkiye. The decision variables for the multi-objective optimization were selected based on engineering feasibility and prior sensitivity analyses. PV and WT capacities were chosen as the primary optimization variables, both constrained within the range of 0.5–10 MW to represent realistic grid-connected system sizes.

In contrast, the Start Hour and Stop Hour parameters were not treated as optimization variables but as scenario-based operational parameters. To investigate the effect of downtime scheduling on the LCOH, multiple fixed off-hour intervals of varying duration (1–8 h per day) were systematically tested across the daily cycle.

This comprehensive time-window analysis enabled the identification of the time periods during which the LCOH reaches its minimum value, revealing the most cost-effective operating schedule for the electrolyzer. By keeping techno-economic sizing (PV–WT) constant, this approach isolates the influence of off-hour duration and timing on overall system performance while ensuring the results reflect realistic grid-price–dependent operation rather than arbitrary time assumptions. The optimization objectives were defined as (i) minimizing the LCOH, and (ii) maximizing the RenFrac, representing the economic and environmental performance of the system, respectively. Although LCOH is often regarded as a result metric, it inherently aggregates CAPEX, OPEX, degradation, and electricity sourcing effects; thus, it can be directly minimized as an economic objective. The RenFrac objective accounts for the renewable share of electricity used for hydrogen generation. In hybrid and grid-connected configurations, maintaining high electrolyser capacity factors may require grid imports, but since the grid mix contains only ~50 % renewable power, this can lower the share of "green" hydrogen. Including RenFrac therefore captures the trade-off between cost efficiency and renewable purity. By simultaneously minimizing LCOH and maximizing RenFrac, the optimization framework ensures that hydrogen production remains both economically viable and environmentally consistent with the intended "green hydrogen" definition, without over-reliance on grid electricity or excessive capital expansion. Among various multi-objective optimization algorithms, MOPSO and NSGA-III were selected to balance exploration and exploitation efficiency. NSGA-III provides strong diversity preservation and Pareto-front accuracy [39], while MOPSO offers fast convergence and fewer control parameters [40]. Other methods such as NSGA-II, SPEA2, and MOEA/D were tested preliminarily but excluded due to slower convergence, weaker diversity, and higher sensitivity to tuning parameters in the context of hybrid renewable–hydrogen system optimization.

2.3.1. Data Acquisition and preprocessing

The surrogate model was trained using a dataset obtained from detailed simulations of a hybrid renewable hydrogen production system. The decision variables were defined as PV capacity (x_1) and WT capacity (x_2), while the outputs included the LCOH and RenFrac. A total of N = 2627 N simulation instances were generated for each case study regions.

Prior to model training, all input and output variables were normalized using min–max scaling to the range [0,1] to improve the numerical stability of neural network training [41]. The normalization is expressed as:

$$x_i^{norm} = \frac{x_i - x_i^{min}}{x_i^{max} - x_i^{min}}, y_j^{norm} = \frac{y_j - y_j^{min}}{y_j^{max} - y_j^{min}} \quad (4)$$

Where x_i^{min}, x_i^{max} and y_j^{min}, y_j^{max} denote the minimum and maximum values of each input and output variable within the training set, respectively. The dataset was randomly divided into training (85 %), validation (15 %), and independent test sets (10 %) using a stratified hold-out procedure [42].

2.3.2. Surrogate model development (artificial neural network)

2.3.2.1. Rationale for surrogate modelling. The high-fidelity simulation of the hybrid PV–WT–PEM electrolyzer system is computationally expensive, especially over a 20-year horizon with hourly resolution (175,200 time steps). Embedding this directly into the optimization loop would make evolutionary algorithms prohibitively slow. To overcome this, a surrogate model (also called a metamodel) was adopted to approximate the input–output mapping at negligible computational cost [43,44].

While alternatives such as Gaussian Process Regression or Kriging are popular in surrogate modelling, they scale poorly when handling thousands of samples in high-dimensional search spaces. An artificial neural network (ANN) was selected instead, as it provides strong nonlinear approximation capabilities, computational efficiency, and scalability for large datasets.

2.3.2.2. Input–output structure. The surrogate model was designed to approximate the nonlinear function:

$$f : R^2 \rightarrow R^3, f(x_1, x_2) = (LCOH, RenFrac) \quad (5)$$

where the decision variables are PV capacity (x_1) and WT capacity (x_2). The outputs correspond to the techno-economic performance indicators generated by the high-fidelity simulation model.

2.3.2.3. Normalization and data preprocessing. All variables were scaled to the unit interval [0,1] using min–max normalization to improve training convergence:

$$x_i^{norm} = \frac{x_i - x_i^{min}}{x_i^{max} - x_i^{min}}, y_j^{norm} = \frac{y_j - y_j^{min}}{y_j^{max} - j^{min}} \quad (6)$$

This ensured comparable magnitudes across variables and preserved monotonic relationships.

2.3.2.4. Artificial neural network architecture. A feedforward multilayer perceptron (MLP) was employed due to its universal function approximation capability [45]. The network architecture consisted of three hidden layers with 64 an 64 neurons, respectively. The hidden layers utilized the hyperbolic tangent sigmoid (tansig) activation function:

$$\sigma(z) = \frac{2}{1 + e^{-2z}} - 1 \quad (7)$$

with the output layer using a linear activation function to maintain the scale of the predicted outputs.

The forward propagation of the ANN can be expressed as:

$$h^{(l)} = \sigma\left(W^{(l)} h^{(l-1)} + b^{(l)}\right), l = 1, 2, 3 \quad (8)$$

$$\widehat{y} = W^{(out)} h^{(3)} + b^{(out)} \quad (9)$$

where $W^{(l)}$ and $b^{(l)}$ denote the weight matrices and bias vectors of the lth layer, and $h^{(0)} = x^{norm}$ is the normalized input vector.

2.3.2.5. Training algorithm. The network weights were optimized using

the Levenberg–Marquardt backpropagation algorithm [46], which updates weights by:

$$\Delta w = -\left(J^T J + \mu I\right)^{-1} J^T e \tag{10}$$

Here, J is the Jacobian of error derivatives with respect to weights, e the error vector, and μ the damping term. It merges the benefits of Gauss–Newton and gradient descent methods., providing fast convergence for medium-sized networks.

The training process aimed to minimize the Mean Squared Error (MSE) loss function:

$$MSE = \frac{1}{N}\sum_{i=1}^{N} \| yi^{norm} - \hat{y}i^{norm} \|^2 \tag{11}$$

Early stopping was applied if validation error failed to improve for 20 epochs.

2.3.2.6. Performance evaluation. Model performance on the test dataset was evaluated using MAE (Mean Absolute Error), RMSE (Root Mean Square Error), and R^2 (Coefficient of Determination) [47]:

$$MAE = \frac{1}{N}\sum_{i=1}^{N} |yi - \hat{y}i|, RMSE = \sqrt{\frac{1}{N}\sum_{i=1}^{N} (yi - \hat{y}i)^2}, R^2 = 1 - \frac{\sum (yi - \hat{y}i)^2}{\sum (yi - \bar{y})^2} \tag{12}$$

The ANN achieved high predictive accuracy, with $R^2 > 0.95$, confirming its suitability as a surrogate for the optimization process.

2.3.3. Multi-objective optimization framework

In order to explore the trade-off between the economic and technical objectives, the problem was formulated as a bi-objective optimization task with decision variables corresponding to PV and WT capacities. The surrogate ANN model was embedded with the aid of two evolutionary algorithms: MOPSO and NSGA-III (See in Fig. 5). Employing two distinct approaches allowed a robustness check of the obtained Pareto fronts and mitigated the risk of algorithm-specific biases, as recommended in comparative multi-objective optimization studies [48].

2.3.3.1. Problem definition. The trained ANN surrogate was integrated into a multi-objective optimization framework. The optimization problem was formulated as:

$$\underset{x \in \Omega}{min}\ F(x) = (f1(x), f2(x)) \tag{13}$$

where decision vector $x = (x1, x2)$,

$$f1(x) = LCOH(x), f2(x) = -RenFrac(x), \tag{14}$$

with the search space Ω = [0.5,10] × [2,8]. The negative sign ensures maximization of RenFrac through minimization.

The optimization aimed at generating a set of non-dominated solutions forming the Pareto front, rather than a single solution. A solution x^a is said to dominate another solution x^b if and only if:

$$\forall_j \in \{1,2\}, f_j(x^a) \le f_j(x^b) \wedge \exists j \in \{1,2\} : f_j(x^a) < fj(x^b) \tag{15}$$

2.3.3.2. Multi-Objective Particle Swarm Optimization. MOPSO extends the classical PSO [49] into multi-objective space by maintaining an external repository of non-dominated solutions [40]. Each particle updates its position and velocity according to Refs. [40,49]:

$$v_i^{t+1} = wv_i^t + c_1 r_1 (p_i - x_i^t) + c_2 r_2 (g - x_i^t) \tag{16}$$

$$x_i^{t+1} = x_i^t + v_i^{t+1} \tag{17}$$

where p_i is the personal best position, g is a leader selected from the repository, w is the inertia weight, and c_1,c_2 are acceleration coefficients

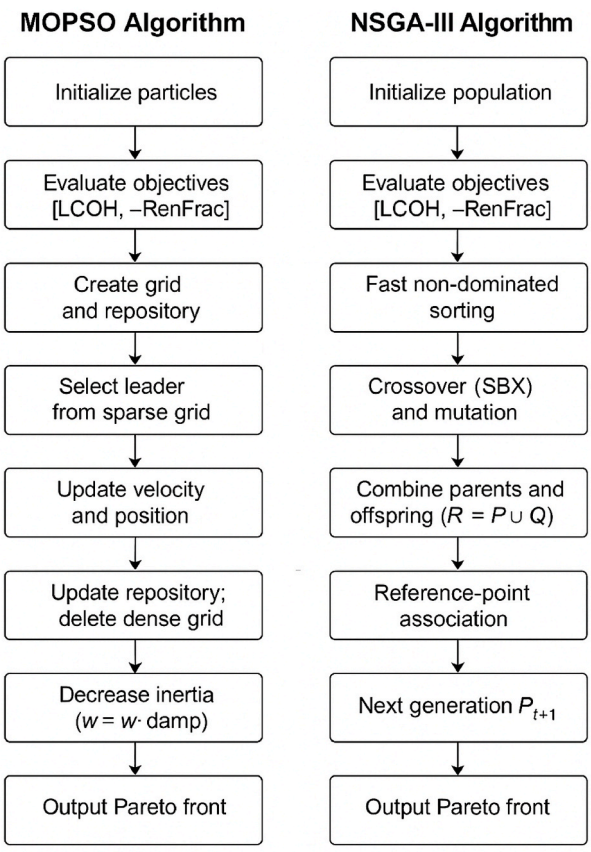

Fig. 5. Flowcharts of the implemented multi-objective optimization algorithms: (a) MOPSO with grid-based leader selection; (b) NSGA-III with SBX crossover and reference-point niching.

with random multipliers r_1, $r_2 \in U(0,1)$. To maintain diversity, the repository is divided into hypercubes (grid cells) in objective space, and leaders are chosen preferentially from less crowded regions using a roulette-wheel mechanism.

Parameter settings: In this study, the swarm size was set to 100 particles, with inertia weight w = 0.5, cognitive/social coefficients c_1 = 1.5, c_2 = 2.0, repository size capped at 50, and inertia damping factor w_{damp} = 0.99. The grid density parameter was set to 10 divisions per objective, with a selection pressure coefficient β = 2. These values are in line with recommended ranges in recent MOPSO applications for energy system optimization [40,50].

2.3.3.3. Non-dominated Sorting Genetic Algorithm III. NSGA-III [39] is a state-of-the-art evolutionary algorithm designed for many-objective optimization. Although the present study considered only two objectives, NSGA-III was selected for its superior diversity-preservation mechanisms based on reference directions. The main steps are.

- Population Initialization – Random solutions uniformly distributed in decision space.
- Variation Operators – Simulated binary crossover (SBX) and polynomial mutation are applied:

$$c_1 = \frac{1}{2}[(1+\beta)p_1 + (1-\beta)p_2],\ c_2 = \frac{1}{2}[(1-\beta)p_1 + (1+\beta)p_2] \tag{18}$$

where β is derived from a distribution index η_c. Mutation perturbs decision variables according to the equation:

$$x_j' = x_j + \delta_j (x_j^{max} - x_j^{min}) \tag{19}$$

where δ_j is drawn from a polynomial distribution with index η_m.

- **Non-dominated Sorting** – Solutions are ranked into Pareto fronts.
- **Niche Preservation** – If the last front exceeds the population size, solutions are selected based on perpendicular distance to predefined reference directions.

Parameter settings: The population size was 100, crossover probability $p_c = 0.9$ with distribution index $\eta_c = 20$, mutation probability $p_m = 0.5$ with $\eta_m = 20$. Sixteen uniformly distributed reference directions were used in the 2D objective space, ensuring an even spread of solutions along the Pareto front.

2.3.3.4. Pareto front analysis and decision-making. The optimization process yielded Pareto fronts for both MOPSO and NSGA-III. To select a single design configuration, the Best Compromise Solution (BCS) was determined using the Closest-to-Utopia approach [51]. The utopia point is defined as the vector of individual objective minima:

$$z^* = (minf1(x), minf2(x)) \tag{20}$$

$$f_j^{norm}(x) = \frac{f_j(x) - f_j^{min}}{f_j^{max} - f_j^{min}}, j = 1, 2 \tag{21}$$

Each Pareto solution was normalized via min–max scaling:
and the Euclidean distance to the utopia point was computed:

$$d(x) = \sqrt{\sum_{j=1}^{2} \left(f_j^{norm}(x)\right)^2} \tag{22}$$

The solution minimizing d(x) was selected as the BCS. This approach ensures a balanced trade-off between economic (LCOH) and technical (RenFrac) objectives.

3. Results and discussion

This study conducted a comparative multi-objective optimization analysis for three distinct locations—Bandırma, Çeşme, and Mersin—using two well-established algorithms: MOPSO and NSGA-III. The primary objectives were to minimize the LCOH and maximize the renewable fraction. Both algorithms were applied to simulation outputs generated by a detailed techno-economic model that incorporates hourly resource variability, system performance, and cost parameters.

3.1. Surrogate model validation and benchmarking

To verify the reliability of the surrogate-based optimization, the ANN model was benchmarked against the full techno-economic simulation using five-fold cross-validation and an out-of-sample error analysis. The network architecture consisted of three hidden layers (64–64–32 neurons) trained with the Levenberg–Marquardt algorithm. Training converged after 434 epochs, reaching a minimum gradient of 9.98×10^{-8} and a mean squared error of 2.38×10^{-10}, indicating excellent convergence stability. The five-fold validation results confirmed very high predictive accuracy across all output variables: MAE = 0.0031 USD kg^{-1} and RMSE = 0.0096 USD kg^{-1} for LCOH, MAE = 0.0001 and RMSE = 0.0003 for the renewable fraction, and MAE = 4.2×10^3 USD and RMSE = 1.1×10^4 USD for total investment. These correspond to sub-percent deviations (<0.5 %) across the feasible design space. Fig. 6 shows the out-of-sample LCOH error distribution across the PV–WT sizing domain. The surface remains nearly flat (<0.05 USD kg^{-1}) for most configurations, with only a small, localized deviation (~0.3 USD kg^{-1}) near under-sampled high-capacity regions. This uniformity demonstrates the surrogate's strong generalization and absence of extrapolation bias. A 95 % confidence-bounded Pareto front (Fig. 6) was further generated by propagating residual errors through the surrogate outputs.

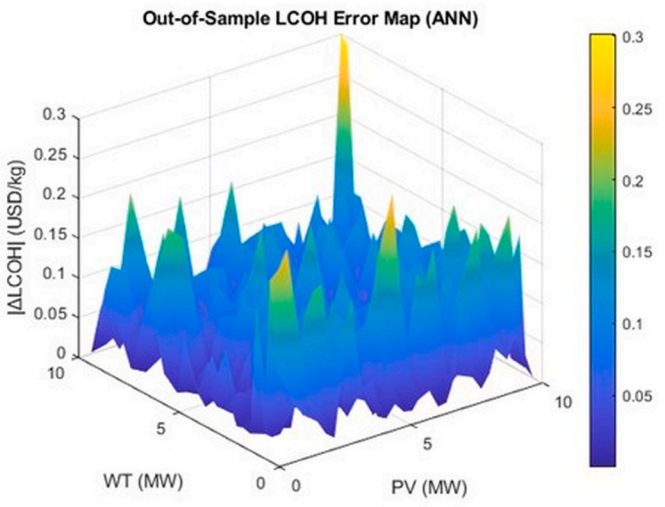

Fig. 6. Out-of-sample LCOH prediction error surface of the trained ANN model.

The resulting confidence bandwidth (<0.1 USD kg^{-1} on LCOH) confirms that the stochastic uncertainty introduced by the ANN model is negligible compared to the inherent techno-economic variability. Overall, these results validate that the ANN surrogate can reliably reproduce the exact model behaviour with several orders-of-magnitude lower computational cost, making it a suitable basis for MOPSO and NSGA-III optimization workflows.

3.2. Algorithmic performance and location-dependent optimization results

The Pareto-optimal fronts generated by each method provided a spectrum of trade-off solutions, from which the BCS was identified based on the minimum Euclidean distance (ED) to the utopia point. Additionally, a k-nearest neighbour (kNN) density metric was used to quantify local Pareto front stability, with higher densities indicating greater robustness to input uncertainties.

Table 4 summarizes the BCS results for each location and algorithm, including the optimal PV and WT capacities, LCOH, RenFrac, ED, and kNN values. In Bandırma, both algorithms achieved a renewable fraction of 0.90, but their outcomes differed in terms of cost and robustness. MOPSO produced an optimal configuration of 2.72 MW PV and 5.85 MW WT, yielding an LCOH of 5.48 USD/kg. Its ED value of 0.46 and relatively low density of 0.033 indicate a stable solution well supported by surrounding Pareto points. NSGA-III, in contrast, achieved a lower LCOH of 5.29 USD/kg with slightly smaller capacities of 2.68 MW PV and 5.59 MW WT, maintaining the same ED. However, its higher density value of 0.113 suggests the solution resides in a less populated region of the Pareto front, implying reduced resilience under fluctuating operating conditions.

In Çeşme, MOPSO again delivered the more robust configuration. With 1.90 MW PV and 5.99 MW WT, it achieved the lowest cost of 5.26 USD/kg alongside a renewable fraction of 0.93. Its ED of 0.44 and density of 0.060 reflect a balanced combination of efficiency and stability. NSGA-III's solution, consisting of 1.69 MW PV and 6.46 MW WT, produced a higher cost of 5.41 USD/kg with the same ED but a denser neighbourhood (0.107). While both achieve strong renewable integration, MOPSO's outcome is more stable, an important consideration in Çeşme where variability in solar and wind profiles makes robustness preferable to marginal cost differences.

The case of Mersin contrasts with the previous two locations, as NSGA-III performed slightly better than MOPSO. The NSGA-III solution, with 4.18 MW PV and 7.14 MW WT, resulted in an LCOH of 6.54 USD/kg and a renewable fraction of 0.85. Its ED of 0.46 and density of 0.111 indicate stronger proximity to the utopia point and greater resilience

Table 4
Comparison of BCS results obtained by MOPSO and NSGA-III across three locations, showing optimal PV and WT capacities, LCOH, RenFrac, ED, kNN density, and validation against Simulink outputs.

Location	Method	PV (MW)	WT (MW)	$LCOH_{BCS}$ ($/kg)	$RenFrac_{BCS}$	ED	kNN	$LCOH_{Sim}$ ($/kg)	$RenFrac_{Sim}$
Bandırma	MOPSO	2.72	5.85	5.48	0.90	0.46	0.033	5.47	0.9
	NSGA-III	2.68	5.59	5.29	0.90	0.46	0.113	5.29	0.9
Çeşme	MOPSO	1.90	5.99	5.26	0.93	0.44	0.060	5.26	0.93
	NSGA-III	1.69	6.46	5.41	0.93	0.44	0.107	5.41	0.93
Mersin	MOPSO	4.04	7.30	6.56	0.85	0.46	0.025	6.56	0.85
	NSGA-III	4.18	7.14	6.54	0.85	0.46	0.111	6.54	0.85

against parameter shifts. By comparison, MOPSO required 4.04 MW PV and 7.30 MW WT to reach a similar renewable fraction but with a higher cost of 6.56 USD/kg and lower density of 0.025. These findings suggest that, under Mersin's relatively steady solar input and moderate wind variability, NSGA-III is more capable of identifying reliable and well-balanced trade-off solutions.

Overall, the comparison highlights the complementary strengths of the two algorithms: MOPSO's superior robustness under fluctuating conditions versus NSGA-III's fine-grained convergence in smoother operating regimes. The observed trends are consistent with reports by Refs. [39,40], who noted that NSGA-III excels in well-behaved Pareto landscapes, while swarm-based methods like MOPSO better preserve diversity and resilience under non-convex or noisy fronts.

The LCOH estimates obtained in this study (5.3–6.5 USD/kg across the modelled regions) show strong consistency with established international benchmarks. According to the IEA's Global Hydrogen Review (2023) [15], typical cost ranges for hybrid renewable hydrogen systems fall between 5.0 and 7.0 USD/kg in mid-resource regions. Curcio (2025) similarly reports values of 5.4–6.6 USD/kg for multi-year dynamic hybrid PV–WT systems [7], while the detailed techno-economic assessment by Terlouw et al. (2022) identifies a range of 5.8–7.2 USD/kg for comparable electrolyzer capacities across various EU locations [52]. The close alignment between these studies and our findings supports the external validity and robustness of the developed modelling framework.

The spatial patterns observed in the Pareto fronts confirm these numerical findings. In Fig. 7a (Bandırma), both algorithms' fronts largely overlap, but MOPSO's BCS is positioned in a denser cluster of solutions, reinforcing its stability advantage. Fig. 7b (Çeşme) shows a similar arrangement, with MOPSO again closer to the utopia point and in a higher-density region. Conversely, Fig. 7c (Mersin) depicts NSGA-III's dominance, with its BCS closer to the utopia point and surrounded by more neighbouring solutions, indicating greater resilience.

Overall, the simulation results demonstrate that algorithm performance is location-dependent: MOPSO tends to provide more stable and reliable solutions in high-variability environments like Bandırma and Çeşme, while NSGA-III performs better in more stable renewable profiles like Mersin. By combining LCOH–RenFrac trade-offs with density-based stability metrics, this study offers a comprehensive basis for selecting optimization strategies tailored to site-specific renewable resource conditions.

For the subsequent in-depth analysis, the Çeşme location optimized with the MOPSO algorithm was selected as the primary case study. This decision is supported by both surrogate-model predictions and simulation validations, which consistently indicated superior performance in terms of techno-economic efficiency and robustness. The MOPSO best-compromise solution (PV = 1.89 kW, WT = 5.9871 kW) achieved an LCOH of 5.26 USD/kg and a renewable fraction of 0.93 in simulation, outperforming the NSGA-III counterpart by yielding a lower cost and a smaller Euclidean distance to the utopia point (ED = 0.44 vs. 0.44). Furthermore, its position within a denser Pareto-front region (kNN = 0.0599) suggests higher local stability against input parameter fluctuations. Given the inherently variable wind and solar resource profiles of Çeşme, this combination of economic advantage, proximity to the ideal solution, and robustness makes the MOPSO–Çeşme configuration the most reliable basis for extended scenario analyses.

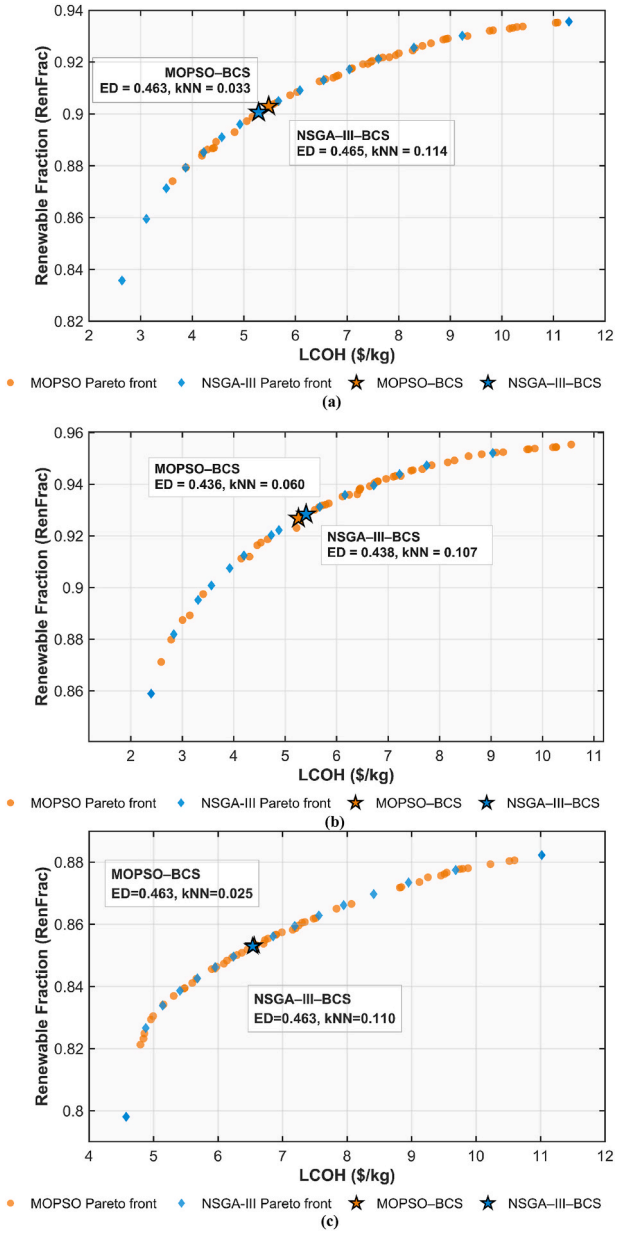

Fig. 7. Pareto fronts for (a) Bandırma, (b) Çeşme, and (c) Mersin, showing MOPSO and NSGA-III BCS with ED and kNN metrics.

3.3. Sensitivity of hydrogen cost to techno-economic parameters

A comparative sensitivity analysis was conducted to evaluate how variations in key techno-economic parameters influence the LCOH

across four system configurations: PV–WT–Grid, PV–Grid, WT–Grid, and Grid-only. A symmetric ±20 % variation range was applied to six input parameters—tax rate, net discount rate (ndr), oxygen by-product price (O_2), distribution capital expenditure (capex_dis), load constraint (load_cons), and degradation coefficient (deg_coef). This range, commonly adopted in renewable hydrogen techno-economic assessments, captures realistic uncertainty bounds linked to market and policy fluctuations while avoiding implausible extrapolations [53–56]. The approach allows direct comparison of parameter sensitivities under consistent perturbation levels, as illustrated in Fig. 8 for the Çeşme case. Across all cases, capex_dis remains the most dominant driver of LCOH fluctuations, indicating that capital investment remains the primary determinant of hydrogen cost. A ±10 % change in capex_dis results in LCOH shifts of approximately ±0.45 USD kg^{-1} H_2 in the PV–WT–Grid system, increasing to nearly ±0.60 USD kg^{-1} H_2 in the Grid-only configuration. The oxygen price shows the second-highest influence, especially in grid-dependent systems where oxygen valorization has higher economic weight. In contrast, tax and deg_coef have negligible effects (<±0.02 USD kg^{-1} H_2), while ndr and load_cons show only moderate sensitivities of about ±0.05 USD kg^{-1} H_2.

Furthermore, the hybrid PV–WT–Grid configuration exhibits not only the lowest LCOH sensitivity but also the highest renewable RenF among all scenarios. This implies that systems integrating both solar and wind generation are more resilient to parameter uncertainties and maintain a more stable cost structure. The flatter slopes observed in Fig. 8 clearly highlight this robustness, confirming that hybrid renewable configurations simultaneously reduce LCOH and enhance the share of renewable energy in hydrogen production, thereby improving the overall sustainability and energy independence of the system.

We monetize stack degradation via an empirically calibrated linear LCOH model.

Four annual degradation fractions were simulated, $d = \{0, 0.5\%, 1.0\%, 1.5\%\}$, yielding LCOH = $\{5.726, 5.823, 5.920, 6.016\}$ USD/kg.

The regression implies a +0.193 USD/kg increase in LCOH per additional +1 %/yr stack degradation. Parametric sweeps show proportional shifts in the optimal PV–WT sizing only when degradation exceeds ~1 %/yr; below that, the capacity plan remains stable, while LCOH shifts almost linearly with *d*. This behavior aligns with the expectation that moderate PEM aging predominantly acts as a levelized cost adder rather than a sizing driver.

3.4. Scale-up effects and economies of scale

To further investigate the role of system scale on the techno-economic feasibility of green hydrogen production, a comparative capacity-scaling analysis was conducted. Fig. 9 compares the LCOH and total investment cost per installed megawatt (Tot INV/MWel) for three different locations—Bandırma, Çeşme, and Mersin—across four electrolyzer capacities (1 MW, 5 MW, 10 MW, and 50 MW). For each capacity, the optimal PV and WT configurations were determined through system simulations, and the corresponding economic performance indicators were computed. Across all locations, both metrics exhibit a clear decreasing trend with increasing electrolyzer capacity, confirming the presence of scale economies. The most pronounced reduction in both LCOH and investment cost occurs when scaling from 1 MW to 5 MW, with diminishing returns observed beyond 10 MW.

In terms of LCOH, Bandırma and Çeşme follow a similar trend, achieving a 35–40 % reduction from 1 MW to 50 MW, while Mersin starts from a higher initial cost (6.54 $/kg) but converges towards the others at larger scales. Regarding investment costs, Mersin generally exhibits slightly higher values, yet the differences among locations become negligible at 50 MW, where costs cluster within a narrow range.

The relative spacing between the LCOH and investment cost curves is largest at low capacities, indicating that small-scale systems suffer from both high unit production costs and high capital intensity. As capacity increases, these curves draw closer and flatten, reflecting reduced marginal cost benefits beyond 50 MW. Overall, the results suggest that installations above 5 MW strike an optimal balance between cost reduction and capacity expansion, while very large-scale systems (>10 MW) offer limited additional economic benefit relative to the required capital outlay. Similar scale-dependent cost behavior has also been reported in the literature. Terlouw et al. [52] demonstrated that large-scale electrolyzer projects benefit from CAPEX dilution and balance-of-plant optimization, with LCOH reductions exceeding 40 % between 1 MW and 20 MW systems. Likewise, Schmidt et al. [57] showed that the learning rate for electrolyzer manufacturing and system integration yields significant cost reductions up to mid-scale plants, after which economies of scale plateau. These studies reinforce that the

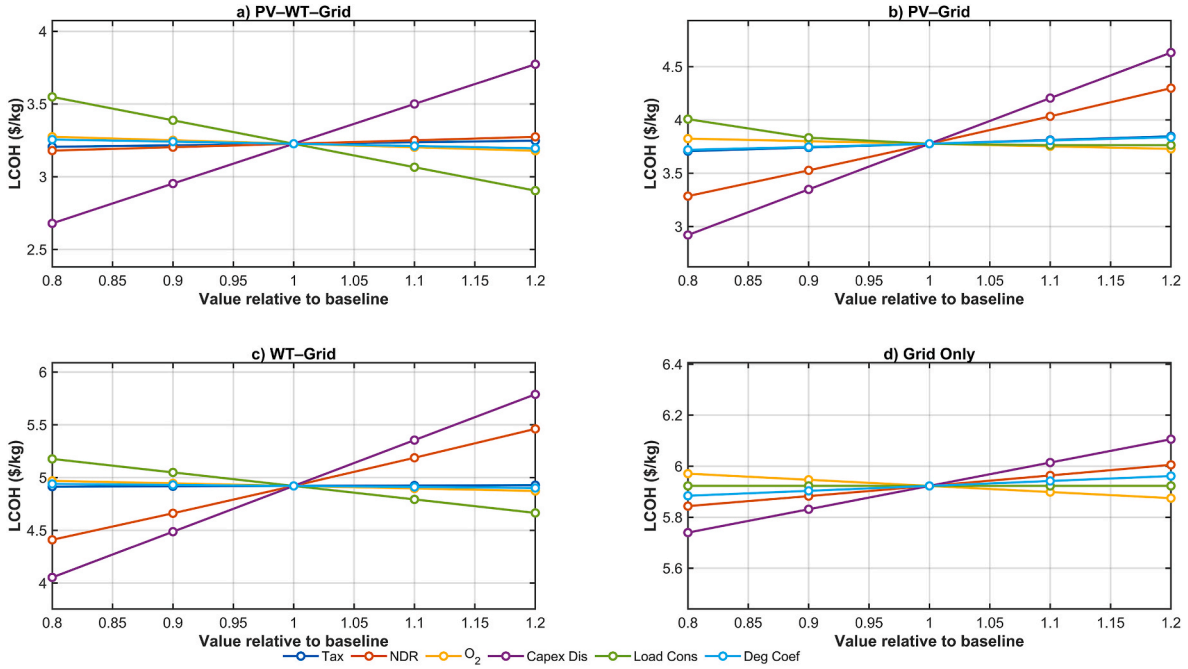

Fig. 8. LCOH sensitivity analysis for Çeşme across taxation, O_2 valorization, CAPEX discount, degradation, and load factors.

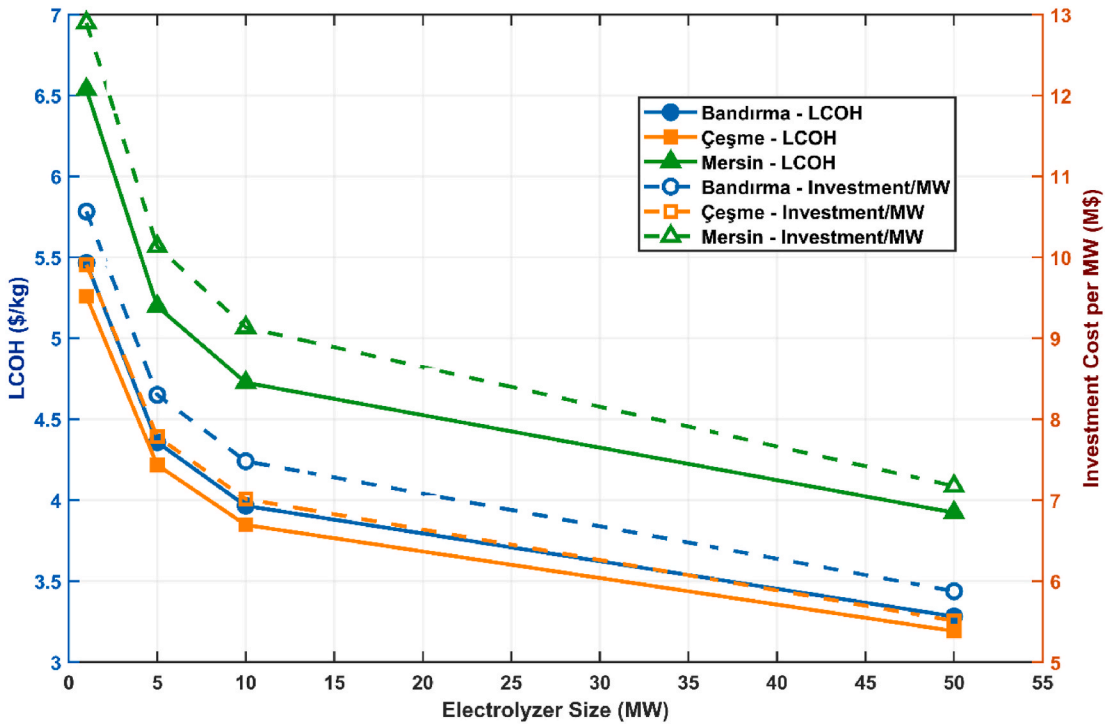

Fig. 9. LCOH and investment cost per MW across electrolyzer capacities (1–50 MW) for Bandırma, Çeşme, and Mersin.

nonlinear relationship between investment cost and hydrogen throughput governs the economic feasibility of scale-up, consistent with the trends observed in the present analysis.

3.5. *Impact of operational scheduling on cost reduction*

To assess the impact of operational downtime on hydrogen production costs, an analysis of off-hour durations and their scheduling was performed. This analysis clearly demonstrates the influence of off-hour durations on the LCOH, as illustrated in Fig. 10. The results show that extending off-hours directly increases LCOH. For instance, with only 1 off-hour per day, the minimum LCOH is 5.67 USD/kg, whereas 8 off-hours per day raise the cost to 8 USD/kg. This finding confirms that downtime is a critical determinant of economic efficiency in hydrogen

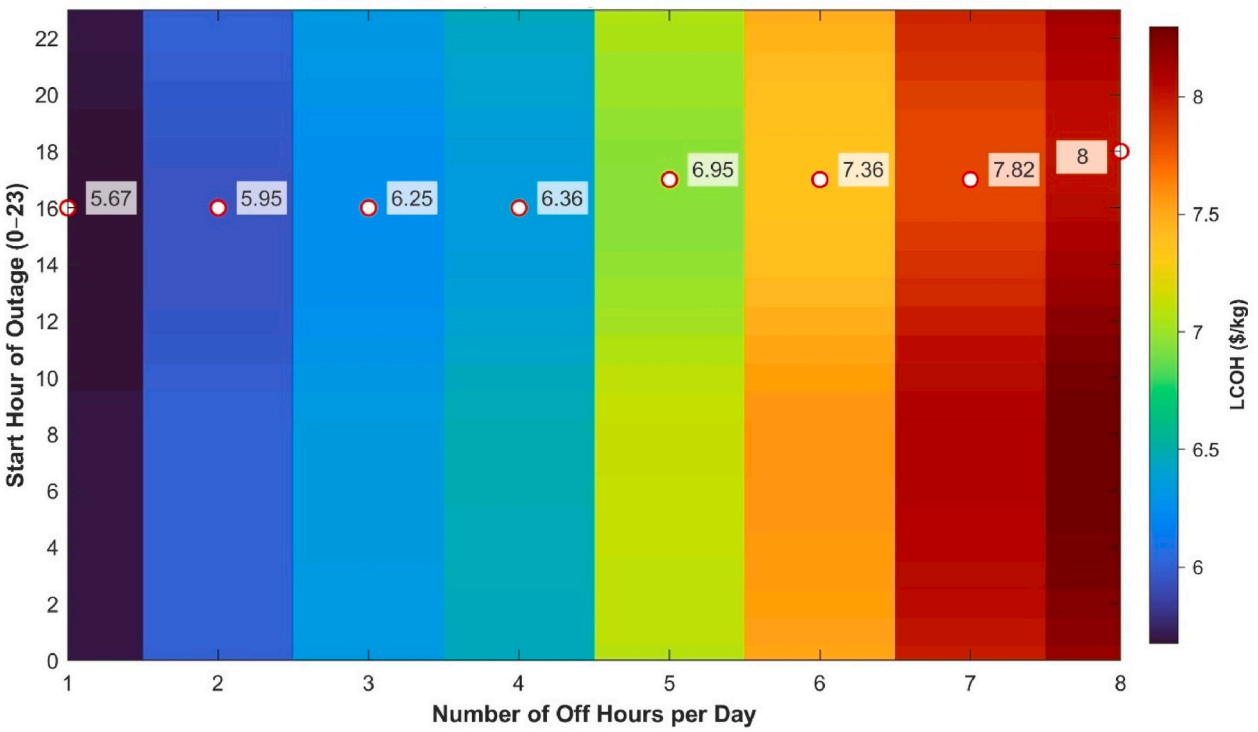

Fig. 10. LCOH sensitivity to off-hour duration and start time for hydrogen production systems.

production systems.

In addition, the starting time of the off-hours also plays a decisive role. In particular, off-periods beginning at 16:00, 17:00, or 18:00 yield the most favourable outcomes. The underlying reason is that these periods coincide with declining solar irradiance and wind speed, while electricity purchase prices rise. Halting production during these hours reduces exposure to high-cost electricity and enhances system-level cost-effectiveness. These findings reinforce previous large-scale techno-economic assessments that identified electricity price variability and renewable resource intermittency as dominant drivers of hydrogen production costs under grid-connected and hybrid configurations [52]. Together, the results provide a quantitative rationale for the strategic scheduling of downtime, showing that careful optimization of both duration and start time is essential to reduce costs and improve system reliability.

3.6. Profitability analysis under market and policy perspectives

Fig. 11 presents the profitability analysis for the Çeşme baseline configuration. Under an 8 % discount rate and 2 % inflation, break-even hydrogen price was identified at ~7.2 USD/kg (NPV ≈ 0; IRR ≈ 8 %). Profitability strengthens above 8 USD/kg, with IRR rising to 12–16 % at 10–12 USD/kg and payback periods compressing to ~6–8 years. These thresholds are highly relevant when compared with current hydrogen market projections: Türkiye's short-term offtake prices are estimated at 7–9 USD/kg, while EU imports are expected to stabilize near 8–10 USD/kg by 2030 [58,59]. This suggests that the modelled systems approach financial viability under realistic policy-driven price signals, particularly when CAPEX reductions and flexible operation are considered.

3.7. Policy sensitivity and fiscal scenario evaluation

Table 5 summarizes the impact of different fiscal policy mechanisms on the techno-economic performance of the optimized PV–WT–PEM system. When benchmarked against the base case, all policy interventions improve the project's financial viability by lowering the LCOH, decreasing the break-even hydrogen selling price, and enhancing investment returns.

The base case yields an LCOH of 4.99 USD kg^{-1}, with a break-even hydrogen price of 7.03 USD kg^{-1}, corresponding to an internal rate of return (IRR) of 8.9 % and a payback period of approximately 9.8 years. This baseline reflects the system performance under current market and fiscal conditions without additional incentives.

Under the reduced corporate income tax scenario, the LCOH decreases marginally by 0.6 %, and the break-even price falls to 6.47 USD kg^{-1}. Although the improvement is modest, the IRR increases to 9.8 % and the payback shortens by roughly one year. The NPV improvement of $+1.54 \times 10^6$ USD indicates that even a small reduction in the tax burden can moderately enhance investment attractiveness.

The carbon credit mechanism (100 USD tCO_2^{-1}) yields a more substantial benefit, reducing the LCOH by 16 % and the break-even price to 6.01 USD kg^{-1}. This corresponds to a net present value gain of $+4.04 \times 10^6$ USD compared to the base case, highlighting the strong leverage of carbon pricing on project economics. The results align with previous findings that carbon revenues can significantly improve the financial sustainability of hydrogen projects (e.g., Gutiérrez-Martín et al., 2020, Energy Conversion and Management, https://doi.org/10.1016/j.enconman.2020.113166).

The Investment Tax Credit (ITC) scenario provides a larger improvement, with the LCOH dropping to 4.06 USD kg^{-1} (−18.5 %), while the break-even hydrogen price declines to 5.79 USD kg^{-1}, enabling an IRR of nearly 9.9 % and a payback period of 8.1 years. The corresponding NPV increase of $+6.03 \times 10^6$ USD demonstrates that upfront capital incentives—by directly reducing the effective CAPEX—are highly effective in improving financial feasibility and accelerating project returns.

Finally, the accelerated depreciation scenario yields the most pronounced economic improvement, achieving an LCOH of 3.82 USD kg^{-1}, corresponding to a 23.6 % cost reduction relative to the base case. By allowing 20 % annual depreciation during the first five fiscal years, the model captures a strong early-stage tax shield effect that increases NPV by $+7.05 \times 10^6$ USD and shortens the payback period to 8 years. This result underscores the efficiency of depreciation-based incentives, which improve project cash flow timing without requiring additional subsidies or direct payments.

Overall, the comparison reveals that ITC and accelerated depreciation provide the highest fiscal leverage among the tested mechanisms, both reducing the LCOH below 4 USD kg^{-1} and improving the IRR to ≈ 10 %. Integrating such fiscal measures into hydrogen techno-economic analyses helps quantify policy-driven competitiveness gains, effectively narrowing the cost gap between green and fossil-based hydrogen by 1.2–1.3 USD kg^{-1}, in line with CBAM-aligned decarbonization

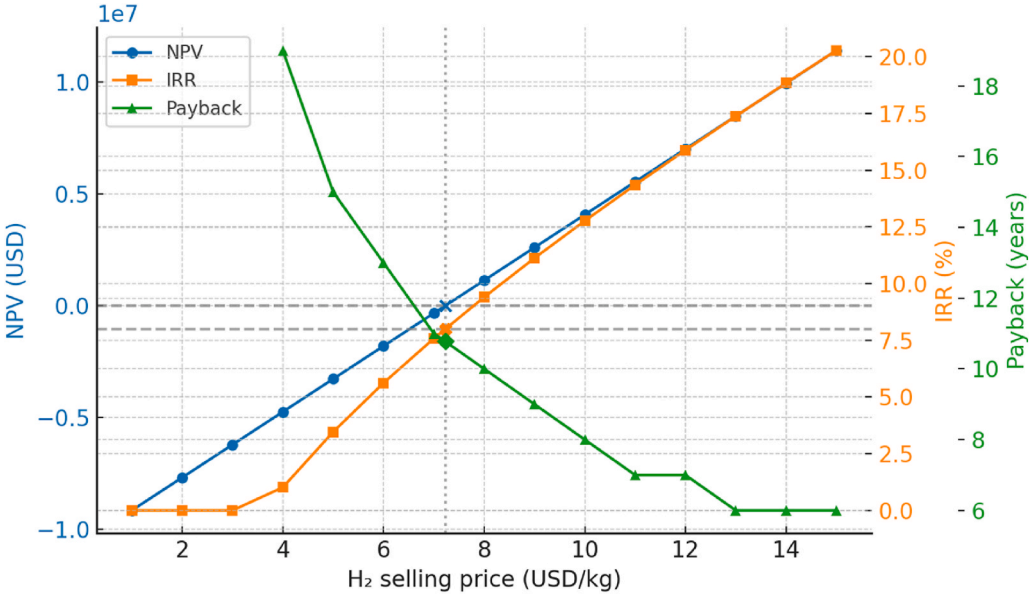

Fig. 11. Profitability metrics versus hydrogen offtake price (Çeşme case).

Table 5
Comparison of LCOH, IRR, and NPV under different fiscal policy scenarios.

Scenario	LCOH (USD/kg)	Δ LCOH (%)	Break-even H_2 price (USD/kg)	IRR (%) @ NPV = 0	Payback (yrs)	Δ NPV vs Base (USD)
Base	4.990	0.00 %	7.03	8.87 %	9.8	–
Reduced corporate income tax	4.960	−0.60 %	6.47	9.84 %	8.9	$+1.54 \times 10^6$
Carbon Credit	4.188	−16.07 %	6.01	8.53 %	9.2	$+4.04 \times 10^6$
Investment Tax Credit (ITC)	4.064	−18.54 %	5.79	9.91 %	8.1	$+6.03 \times 10^6$
Accelerated depreciation	3.816	−23.6 %	5.42	9.78 %	8	$+7.05 \times 10^6$

frameworks.

The fiscal elements used in the CBAM-aligned scenario are intended to approximate the types of support measures currently being discussed or implemented in the EU and Türkiye, rather than to replicate any specific policy. The Investment Tax Credit (ITC) in the model reflects a general form of upfront capital relief that is mentioned in several international assessments, including the IEA's Global Hydrogen Review (2023), as one of the tools used to reduce early CAPEX burdens for clean-energy projects. Likewise, the accelerated depreciation assumption is broadly consistent with the structure of Türkiye's existing investment incentive framework, which allows certain technologies to benefit from shortened amortization periods. While these mechanisms do not correspond directly to any single regulation, they help place the scenario within a plausible policy environment and provide a reasonable basis for exploring how supportive fiscal conditions might influence project economics under CBAM-related dynamics.

3.8. Comparative techno-economic assessment of hydrogen storage options

To quantify the techno-economic implications of alternative hydrogen storage pathways, five storage configurations were compared under identical production and grid conditions: no storage, compressed hydrogen at 350 bar and 700 bar, liquid organic hydrogen carrier (LOHC), and cryogenic liquid hydrogen (LH_2). Fig. 12 illustrates the resulting LCOH, break-even selling price, and payback period.

The base (no-storage) case achieves an LCOH of 4.99 USD kg^{-1} with a break-even H_2 price of 7.19 USD kg^{-1} and a payback period of 10.8 years.

Compressed hydrogen options increase the total cost due to higher compression energy and vessel CAPEX: +9.8 % for 350 bar and +12.5 % for 700 bar storage, resulting in LCOHs of 5.48–5.62 USD kg^{-1} and slightly longer payback periods (≈11 years).

In contrast, the LOHC route offers a moderate LCOH increase to 5.03 USD kg^{-1}, despite additional conversion energy and catalyst replacement costs, because it avoids high-pressure storage and benefits from lower safety requirements and simpler logistics.

Finally, the cryogenic LH_2 system exhibits the highest LCOH (7.92 USD kg^{-1}) and selling price (11.35 USD kg^{-1}), reflecting its significant liquefaction energy demand (~10 kWh kg^{-1}) and high insulation CAPEX, though it maintains a competitive payback time (10.6 years) due to large-scale operational efficiency.

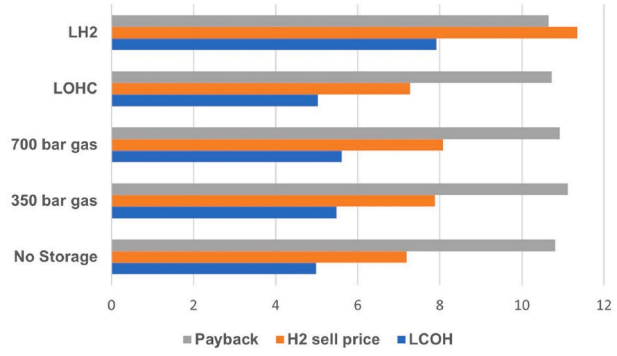

Fig. 12. Comparison of LCOH, break-even H_2 selling price, and payback period for different hydrogen storage options.

Overall, the comparison demonstrates that while compressed gas and LOHC systems offer moderate cost increases (5–20 %) compared to direct use, cryogenic storage nearly doubles energy-related costs but remains relevant for large-scale export applications due to high volumetric density and transport compatibility. These trends are consistent with the findings of Cardella (2018), Gutiérrez-Martín et al. (2020), and Yang & Lee (2021), who similarly reported energy penalties of 8–12 kWh kg^{-1} and LCOH increments of 30–60 % for LH_2 pathways.

4. Conclusions

This study presents a comprehensive techno-economic framework for evaluating renewable-based hydrogen production using long-term dynamic simulation and multi-objective optimization. By integrating degradation effects, water sourcing, storage alternatives, fiscal incentives, and market-driven electricity dynamics into a 20-year modelling horizon, the study provides a realistic view of cost evolution under Türkiye's policy and resource conditions.

The main findings of this study can be summarized as follows.

1. System scale and resource availability strongly influence hydrogen costs. Hybrid PV–WT systems achieve up to 40 % LCOH reduction when scaled from 1 MW to 50 MW, with the most cost-effective outcomes observed in wind-rich regions such as Çeşme and Bandırma.
2. Algorithmic performance is location-dependent. MOPSO generally provides more robust configurations under high renewable variability, whereas NSGA-III performs slightly better in solar-dominant regions with smoother profiles, such as Mersin.
3. Operational flexibility has a measurable economic impact. Strategically aligning electrolyzer downtime with evening high-price periods improves competitiveness by reducing LCOH by up to 10 %, highlighting the value of market-aware scheduling.
4. Fiscal incentives substantially improve project feasibility. Investment Tax Credits and accelerated depreciation reduce LCOH by 18–24 %, demonstrating strong alignment with CBAM-driven decarbonization pathways and reinforcing the importance of policy support for early-stage hydrogen markets.

Overall, the study's contribution lies in presenting an integrated and applied techno-economic framework that brings together long-term dynamic behaviour, component degradation, water sourcing and treatment considerations, hydrogen storage options, and hourly market-based operation within a unified 20-year assessment. Rather than proposing new modelling methods, the framework integrates well-established tools in a policy-relevant context suited to Türkiye's emerging hydrogen sector.

Despite its comprehensive scope, the study has several limitations. The degradation of system components was modelled using fixed annual rates, without considering random failures or maintenance interruptions. The economic analysis was limited to the Turkish market structure and static policy assumptions; future fluctuations in electricity prices or taxation could change the results. Moreover, the environmental dimension was restricted to CO_2 emissions from grid imports, excluding

a full life cycle or transport assessment. These simplifications were necessary to keep the model computationally tractable but inevitably constrain the generality of the results.

Future work should therefore aim to incorporate stochastic and real-time operation data to capture uncertainty more accurately. Expanding the framework to include alternative electrolyzer technologies (such as AEM or SOEC), sector-coupling scenarios, and life-cycle carbon accounting would provide a more complete picture of green hydrogen competitiveness. Integration with grid-scale energy management or adaptive control strategies through data-driven models could also help align techno-economic optimization with real operational behaviour.

Although the case studies focus on Türkiye, the modelling approach is broadly applicable to other emerging hydrogen markets—particularly in MENA and South America—where similar renewable profiles, cost structures, and policy transitions are driving interest in CBAM-aligned green hydrogen pathways.

CRediT authorship contribution statement

Metin Gül: Writing – review & editing, Writing – original draft, Visualization, Validation, Software, Methodology, Data curation. **Ersin Akyüz:** Writing – review & editing, Validation, Supervision, Project administration, Conceptualization.

Declaration of competing interest

The authors declare that they have no known competing financial interests or personal relationships that could have appeared to influence the work reported in this paper.

The author is an Editorial Board Member/Editor-in-Chief/Associate Editor/Guest Editor for this journal and was not involved in the editorial review or the decision to publish this article.

The authors declare the following financial interests/personal relationships which may be considered as potential competing interests.

Acknowledgement

The authors would like to acknowledge the financial support provided by Balıkesir University Research Project (BAP) under Grant No. 2025-196.

Appendix A. Supplementary data

Supplementary data to this article can be found online at https://doi.org/10.1016/j.ijhydene.2025.153172.

References

[1] Carapellucci R, Giordano L. Modeling and optimization of an energy generation island based on renewable technologies and hydrogen storage systems. Int J Hydrogen Energy 2012;37:2081–93. https://doi.org/10.1016/j.ijhydene.2011.10.073.
[2] McIlwaine N, Foley AM, Morrow DJ, Al Kez D, Zhang C, Lu X, et al. A state-of-the-art techno-economic review of distributed and embedded energy storage for energy systems. Energy 2021;229:120461. https://doi.org/10.1016/j.energy.2021.120461.
[3] Maestre VM, Ortiz A, Ortiz I. Challenges and prospects of renewable hydrogen-based strategies for full decarbonization of stationary power applications. Renew Sustain Energy Rev 2021;152:111628. https://doi.org/10.1016/j.rser.2021.111628.
[4] Undertaking FC. H2J. Hydrogen roadmap Europe : a sustainable pathway for the European energy transition. Publications Office; 2019.
[5] Kayfeci M, Keçebaş A, Bayat M. Hydrogen Production 2019:45–83. https://doi.org/10.1016/B978-0-12-814853-2.00003-5.
[6] Bauer C, Desai H, Heck T, Sacchi R, Schneider S, Terlouw T, et al. Electricity storage and hydrogen – technologies, costs and impacts on climate change. 2022.
[7] Bourne S. The future of fuel: the future of hydrogen. Fuel Cell Bull 2012;2012:12–5. https://doi.org/10.1016/S1464-2859(12)70027-5.
[8] Schmidt O, Gambhir A, Staffell I, Hawkes A, Nelson J, Few S. Future cost and performance of water electrolysis: an expert elicitation study. Int J Hydrogen Energy 2017;42:30470–92. https://doi.org/10.1016/j.ijhydene.2017.10.045.
[9] Akyuz E, Tezer T. Techno-economic feasibility and regression analysis of green hydrogen production from solar and wind energy in Türkiye. Int J Hydrogen Energy 2025;142. https://doi.org/10.1016/j.ijhydene.2025.02.151.
[10] Ramsebner J, Linares P, Hiesl A, Haas R. Techno-economic evaluation of renewable hydrogen generation strategies for the industrial sector. Int J Hydrogen Energy 2024;60:1020–40. https://doi.org/10.1016/j.ijhydene.2024.02.167.
[11] Restelli F, Spatolisano E, Pellegrini LA, Cattaneo S, de Angelis AR, Lainati A, et al. Liquefied hydrogen value chain: a detailed techno-economic evaluation for its application in the industrial and mobility sectors. Int J Hydrogen Energy 2024;52:454–66. https://doi.org/10.1016/j.ijhydene.2023.10.107.
[12] Kroniger D, Madlener R. Hydrogen storage for wind parks: a real options evaluation for an optimal investment in more flexibility. Appl Energy 2014;136:931–46. https://doi.org/10.1016/j.apenergy.2014.04.041.
[13] Jung HY. Techno-economic analysis of hybrid energy storage system with renewable energy coupling hydrogen technology. https://doi.org/10.20944/preprints202307.1281.v1; 2023.
[14] Gül M, Akyüz E. Techno-economic viability and future price projections of photovoltaic-powered green hydrogen production in strategic regions of Turkey. J Clean Prod 2023;430:139627. https://doi.org/10.1016/j.jclepro.2023.139627.
[15] Hosseini SE, Wahid MA. Hydrogen production from renewable and sustainable energy resources: promising green energy carrier for clean development. Renew Sustain Energy Rev 2016;57:850–66. https://doi.org/10.1016/j.rser.2015.12.112.
[16] Parkinson B, Balcombe P, Speirs JF, Hawkes AD, Hellgardt K. Levelized cost of CO2 mitigation from hydrogen production routes. Energy Environ Sci 2019;12:19–40. https://doi.org/10.1039/C8EE02079E.
[17] (IEA) IEA. Global hydrogen review 2024. International Energy Agency; 2024.
[18] María Villarreal Vives A, Wang R, Roy S, Smallbone A. Techno-economic analysis of large-scale green hydrogen production and storage. Appl Energy 2023;346:121333. https://doi.org/10.1016/j.apenergy.2023.121333.
[19] Curcio E. Techno-economic analysis of hydrogen production: costs, policies, and scalability in the transition to net-zero. Int J Hydrogen Energy 2025;128:473–87. https://doi.org/10.1016/j.ijhydene.2025.04.013.
[20] Schofield L, Paren B, Macdonald R, Shao-Horn Y, Mallapragada D. Dynamic optimization of proton exchange membrane water electrolyzers considering usage-based degradation. AIChE J 2024;71. https://doi.org/10.1002/aic.18635.
[21] Simoes SG, Catarino J, Picado A, Lopes TF, di Berardino S, Amorim F, et al. Water availability and water usage solutions for electrolysis in hydrogen production. J Clean Prod 2021;315:128124. https://doi.org/10.1016/j.jclepro.2021.128124.
[22] Teske F, Schubert J, Fehrle A, Funk F, Franke J. Techno-economic analysis of battery storage systems and hydrogen-based storage systems as an alternative to grid expansion in the medium voltage grid in Germany. AIMS Energy 2023;11:358–401. https://doi.org/10.3934/energy.2023019.
[23] Ahmed R, Shehab SA, Elzeki OM, Darwish A, Hassanein AE. An explainable AI for green hydrogen production: a deep learning regression model. Int J Hydrogen Energy 2024;83:1226–42. https://doi.org/10.1016/j.ijhydene.2024.08.064.
[24] Tariq AH, Anwar M, Abbas Kazmi SA, Hassan M, Bahadar A. Techno-economic and composite performance assessment of fuel cell-based hybrid energy systems for green hydrogen production and heat recovery. Int J Hydrogen Energy 2025;104:444–62. https://doi.org/10.1016/j.ijhydene.2024.04.018.
[25] Jung H. Techno-economic analysis of hybrid energy storage system with renewable energy coupling hydrogen technology. https://doi.org/10.20944/preprints202307.1281.v1; 2023.
[26] Simoes SG, Catarino J, Picado A, Lopes TF, di Berardino S, Amorim F, et al. Water availability and water usage solutions for electrolysis in hydrogen production. J Clean Prod 2021;315:128124. https://doi.org/10.1016/j.jclepro.2021.128124.
[27] Simulink MathWorks. Simulation and model-based design. 2024.
[28] NASA POWER Project. Prediction of worldwide energy resources (POWER) data access viewer & API. 2025.
[29] (IRENA) IREA. Sector coupling in facilitating integration of variable renewable energy in cities. Abu Dhabi: International Renewable Energy Agency; 2021.
[30] IRENA. Green hydrogen cost reduction: scaling up electrolysers to meet the 1.5 °C climate goal. Abu Dhabi. 2020.
[31] Okonkwo PC, Nwokolo SC, Meyer EL, Ahia CC, Mansir IB. Techno-economic optimization of renewable hydrogen infrastructure via AI-based dynamic pricing. Sci Rep 2025;15:31529. https://doi.org/10.1038/s41598-025-17506-z.
[32] Yang T, Yan X, Cai W, Luo H, Xu N, Tong L, et al. Parametric study and optimization of hydrogen production systems based on solar/wind hybrid renewable energies: a case study in kuqa, China. Sustainability 2024;16:896. https://doi.org/10.3390/su16020896.
[33] Tezer T, Akyuz E, Gul M. Optimal and reliable design of stand-alone hybrid renewable energy systems: a multi-objective approach. Energy Sources, Part A Recovery, Util Environ Eff 2024;46:10948–63. https://doi.org/10.1080/15567036.2024.2378482.
[34] Hong S, Lee J, Cho H, Kim M, Moon I, Kim J. Multi-objective optimization of CO2 emission and thermal efficiency for on-site steam methane reforming hydrogen production process using machine learning. J Clean Prod 2022;359:132133. https://doi.org/10.1016/j.jclepro.2022.132133.
[35] Ishaq H, Dincer I. Multi-objective optimization and analysis of a solar energy driven steam and autothermal combined reforming system with natural gas. J Nat Gas Sci Eng 2019;69:102927. https://doi.org/10.1016/j.jngse.2019.102927.
[36] Cao Y, Alsharif S, Attia E-A, Shamseldin MA, Ibrahim BF. A conceptual process design towards CO2 emission reduction by integration of solar-based hydrogen production and injection into biomass-derived solid oxide fuel cell. Process Saf Environ Prot 2022;164:164–76. https://doi.org/10.1016/j.psep.2022.05.050.
[37] Shboul B, Zayed ME, Tariq R, Ashraf WM, Odat A-S, Rehman S, et al. New hybrid photovoltaic-fuel cell system for green hydrogen and power production:

performance optimization assisted with gaussian process regression method. Int J Hydrogen Energy 2024;59:1214–29. https://doi.org/10.1016/j.ijhydene.2024.02.087.
[38] Das S, De S, Dutta R, De S. Multi-criteria decision-making for techno-economic and environmentally sustainable decentralized hybrid power and green hydrogen cogeneration system. Renew Sustain Energy Rev 2024;191:114135. https://doi.org/10.1016/j.rser.2023.114135.
[39] National Renewable Energy Laboratory (NREL). Utility-scale PV — annual technology baseline 2024. 2024.
[40] National Renewable Energy Laboratory (NREL). Land-based wind — annual technology baseline 2024. 2024.
[41] Galletti A, Pasimeni F, Melideo D, Desideri U, Alkemade F. Learning in green hydrogen production: insights from a novel European dataset. Int J Hydrogen Energy 2025;148:149812. https://doi.org/10.1016/j.ijhydene.2025.06.002.
[42] Bellotti D, Rivarolo M, Magistri L. A comparative techno-economic and sensitivity analysis of Power-to-X processes from different energy sources. Energy Convers Manag 2022;260:115565. https://doi.org/10.1016/J.ENCONMAN.2022.115565.
[43] Connelly E, Penev M, Elgowainy A, Hunter C. Current status of hydrogen liquefaction costs. 2019.
[44] Falama RZ, Soulouknga MH, Dumbrava V, Salah A. Renewable energy systems for hydrogen production in Sub-Saharan Africa: a comparative study based on a techno-economic analysis. UPB Scientific Bulletin, Series C: Electrical Engineering and Computer Science 2023;85:351–64.
[45] Simoes SG, Catarino J, Picado A, Lopes TF, di Berardino S, Amorim F, et al. Water availability and water usage solutions for electrolysis in hydrogen production. J Clean Prod 2021;315:128124. https://doi.org/10.1016/j.jclepro.2021.128124.
[46] T.C. Enerji ve Tabii Kaynaklar Bakanlığı. Elektrik Üretimi ve Elektrik tüketim noktası emisyon faktörleri. 2024.
[47] Deb K, Jain H. An evolutionary many-objective optimization algorithm using reference-point-based nondominated sorting approach, part I: solving problems with box constraints. IEEE Trans Evol Comput 2014;18:577–601. https://doi.org/10.1109/TEVC.2013.2281535.
[48] Coello CAC, Pulido GT, Lechuga MS. Handling multiple objectives with particle swarm optimization. IEEE Trans Evol Comput 2004;8:256–79. https://doi.org/10.1109/TEVC.2004.826067.
[49] Goodfellow I, Bengio Y, Courville A. Deep learning. MIT Press; 2016.
[50] Kohavi R. A study of cross-validation and bootstrap for accuracy estimation and model selectionvol. 14; 2001.
[51] Forrester AIJ, Keane AJ. Recent advances in surrogate-based optimization. Prog Aero Sci 2009;45:50–79. https://doi.org/10.1016/j.paerosci.2008.11.001.
[52] Queipo NV, Haftka RT, Shyy W, Goel T, Vaidyanathan R, Kevin Tucker P. Surrogate-based analysis and optimization. Prog Aero Sci 2005;41:1–28. https://doi.org/10.1016/j.paerosci.2005.02.001.
[53] Hornik K, Stinchcombe M, White H. Multilayer feedforward networks are universal approximators. Neural Netw 1989;2:359–66. https://doi.org/10.1016/0893-6080(89)90020-8.
[54] Hagan MT, Menhaj MB. Training feedforward networks with the marquardt algorithm. IEEE Trans Neural Netw 1994;5:989–93. https://doi.org/10.1109/72.329697.
[55] Bagheri B, Kumagai H, Hashimoto M, Sugiyama M. Techno-economic assessment of green hydrogen production in Australia using off-grid hybrid resources of solar and wind. Energies 2025;18:3285. https://doi.org/10.3390/en18133285.
[56] Fernandes L, Machado F, Marcon L, Fonseca A. Unified case study analysis of techno-economic tools to study the viability of off-grid hydrogen production plants. Hydrogen 2025;6:72. https://doi.org/10.3390/hydrogen6030072.
[57] Willmott C, Matsuura K. Advantages of the mean absolute error (MAE) over the root mean square error (RMSE) in assessing average model performance. Clim Res 2005;30:79–82. https://doi.org/10.3354/cr030079.
[58] Ishibuchi H, Tsukamoto N, Nojima Y. Evolutionary many-objective optimization: a short review. 2008 IEEE congress on evolutionary computation. IEEE World Congress on Computational Intelligence); 2008. p. 2419–26. https://doi.org/10.1109/CEC.2008.4631121.
[59] Kennedy J, Eberhart R. Particle swarm optimization. Proceedings of ICNN'95 - International Conference on Neural Networks 1995;4:1942–8. https://doi.org/10.1109/ICNN.1995.488968.